

# Can gas dynamics in centres of galaxies reveal orbiting massive black holes?

James Etherington and Witold Maciejewski

*Astrophysics, Denys Wilkinson Building, Keble Road, Oxford OX1 3RH*

19 September 2018

## ABSTRACT

If supermassive black holes in centres of galaxies form by merging of black-hole remnants of massive Population III stars, then there should be a few black holes of mass one or two orders of magnitude smaller than that of the central ones, orbiting around the centre of a typical galaxy. These black holes constitute a weak perturbation in the gravitational potential, which can generate wave phenomena in gas within a disc close to the centre of the galaxy. Here we show that a single orbiting black hole generates a three-arm spiral pattern in the central gaseous disc. The density excess in the spiral arms in the disc reaches values of 3–12% when the orbiting black hole is about ten times less massive than the central black hole. Therefore the observed density pattern in gas can be used as a signature in detecting the most massive orbiting black holes.

**Key words:** hydrodynamics — galaxies: kinematics and dynamics — galaxies: spiral — galaxies: structure — galaxies: nuclei — cosmology: dark matter

## 1 INTRODUCTION

Numerical simulations of structure formation indicate that baryonic cores within dark matter haloes collapse at redshifts  $z \approx 20 - 30$  to sufficiently high densities to be available for primordial star formation (e.g. Abel et al 1998). Because of the lack of metals that could facilitate cooling, the collapse occurs without much fragmentation and it gives rise to the Population III stars, much more massive than stars forming today (Abel, Bryan & Norman 2000). Stars as massive as  $10^3 M_{\odot}$  could form, and they could evolve into massive black holes (MBHs) with little mass loss (Madau & Rees 2001). A Population III star with a mass greater than  $260 M_{\odot}$  will not experience a supernova explosion, because the gravity of the star is too strong, and instead it will simply collapse to form a black hole. Islam, Taylor & Silk (2003, 2004a) followed in detail hierarchical merging of such a population of primordial black holes, and they found that about  $10^3$  MBHs would be present in the galactic halo today. In total, mass comparable or greater than that of the central supermassive black hole (SMBH) should still reside in MBHs orbiting in galactic halos. Most of these MBHs would have masses near the initial seed mass of the remnant Population III star, but there would be a few as massive as  $10^6 - 10^7 M_{\odot}$ .

In this paper we investigate whether the most massive MBHs orbiting in galactic halos can be revealed by structures related to waves that they generate in gaseous discs in centres of galaxies. At the nuclear scales, gas dynamics becomes decoupled from dynamics of the stars, and one can study the response of the former to any imposed gravitational potential. A linear theory applicable here was developed by Goldreich & Tremaine (1978, 1979), who showed that density waves can propagate within the gas as a re-

sponse to a rigidly rotating potential. The propagation of waves depends crucially on the resonances created by the rotating potential, since waves are generated at these resonances. Waves propagating in gas generate spiral structure there, and the linear theory was first invoked by Lindblad & Jörsäter (1981) to explain the spiral structure observed in the centre of a barred galaxy. Maciejewski (2004 a,b) used the linear theory and hydrodynamical modelling to analyse nuclear spirals generated by a wide range of galactic potentials, including ones that have a SMBH at the centre and a bisymmetric bar. These latter papers suggest that asymmetries in the galactic potential too weak to be detected observationally might be sufficient to generate nuclear spirals that should be easily observed.

A single MBH orbiting in the galactic halo gives rise to an asymmetric perturbation in the potential rather than to a bisymmetric one, caused by a bar, that has been studied previously. In this paper we investigate in detail gas dynamics generated by this potential using hydrodynamical modelling. There are similarities here to the interaction between a protoplanet and the protostellar disc (e.g. Lin & Papaloizou 1993), although there are also significant differences which we point out.

The structure of the paper is as follows. Section 2 presents the numerical code, the gravitational potential and the parameters used. All of the models are summarized in Table 1, and in Section 3 representative models are analyzed further. An interpretation of the results is given in Section 4. Implications of the models for the detection of MBHs orbiting in galaxies, and other detection methods are discussed in Section 5. We summarize our conclusions in Section 6.

## 2 METHODOLOGY

The modelling of gas dynamics was performed using the CMHOG2 code that was developed from the original CMHOG code by Piner, Stone & Teuben (1995). The code solves the hydrodynamical fluid equations on a log-polar grid in two dimensions. The PPM scheme is employed and the gas is assumed to be isothermal. Each time-step the code calculates three hydrodynamical variables: the radial and tangential components of the gas velocity and the gas density. By modifying appropriate subroutines it is possible to model the gas in practically any gravitational potential desired. The data files that the code creates can be used to study the time evolution of the gas, investigate the structure and dynamics of gas and search for stable patterns in gas flow. The log-polar grid extends from an inner radius of 5 pc to an outer radius at 4 kpc, which is large enough to encircle all wave phenomena. At the outer boundary the waves have effectively decayed completely so reflections there are insignificant. We use closed boundary (reflection) conditions at both the inner and outer ends of the grid. The grid consists of 174 radial annuli that are split by 160 angular slices. The grid is logarithmic, with the smallest cells at the inner boundary, to make the cells approximately square. The cell size at the inner boundary is 0.19 pc, which allows the central region to be examined in great detail, and at the outer boundary it is 160 pc.

The code uses Athanasoulas's (1992) model of the galactic potential which originally had two components: the disc and the bulge. Following Maciejewski (2004b) we added a central SMBH. The disc has a surface density of the form:  $\sigma(R) = \sigma_0(1 + R^2/R_0^2)^{-3/2}$ , which requires two parameters: the surface density at the centre of the disc  $\sigma_0$  and a characteristic radius  $R_0$ . The bulge has a volume density:  $\rho(r) = \rho_b(1 + r^2/r_0^2)^{-3/2}$ . Similarly, it requires two free parameters: the density at the centre of the bulge  $\rho_b$  and a characteristic radius  $r_0$ . All four parameters are taken from Athanasoulas's standard model. The SMBH is modelled using Plummer's formula, which ensures that there is no singularity at its location. The mass of the SMBH is  $10^8 M_\odot$  throughout this work, which corresponds to 0.65% of the mass within the inner 1 kpc from the centre, and the softening is 0.01 kpc.

For the purpose of this work a subroutine was created to simulate either one or two MBHs orbiting the galactic centre. As a first step, we studied gas response to two equal MBHs, one being a mirror symmetry of the other. This situation, although unphysical, can be directly compared to simulations of gas flow in bars because of its bisymmetry. In all our models one or two MBHs follow a circular orbit with a 1 kpc radius. The MBH mass was set to  $10^6$ ,  $10^7$  or  $10^8 M_\odot$ . The first two values correspond to the most massive MBHs that may orbit around the centres of galaxies. The last value, although unphysical, was used to estimate how the density contrast in gas changes with the MBH mass. Plummer's formula was used again to soften the MBH mass distribution, but this time the softening was set to 10, 50 or 100 pc. On the grid used, the cell size at 1 kpc is 40 pc. The orbiting MBHs are not permitted to accrete gas in the sense that there is no loss of gas from the grid at the location of the MBHs. However, in the softened potential of a Plummer sphere, there is still a possibility that the disc gas may be captured by the orbiting MBH.

The hydrodynamical simulations were initially performed in a frame rotating with the MBHs located in the galactic plane. Later the code was modified to follow the MBHs orbiting in a stationary frame. The second method was advantageous since it allowed us to study orbital motion out of the plane of the galaxy, for which the projection of the MBH on the galactic plane moves with changing

angular speed. To check for consistency, models with MBHs orbiting in the galactic plane were created with the two versions of the code. The outputs showed no detectable differences.

The orbital period at a radial distance of 1 kpc is about 20 Myrs. To ensure that the response of the gas was smooth, the mass of the off-centre MBHs was introduced gradually during the first orbit. To obtain the steady state response of the gas the models were run for 100 Myrs. This corresponds to about 5 orbits, which was long enough to recover all relevant structures in gas. The sound speed in gas in the models is  $20 \text{ km s}^{-1}$ , which is typical for gas velocity dispersion in the inner parts of galaxies. A wave in such gas can propagate a distance of 2 kpc in 100 Myrs. Thus the wave has enough time to cross the area encircled by the MBH's orbit within the time of the run.

## 3 RESULTS

In total we built 29 models, for which we varied four parameters: the number of orbiting MBHs, the inclination of their orbit with respect to the galactic plane, as well as the mass and softening of the orbiting MBHs. The models together with their parameters are presented in Table 1. Below we analyze representative models.

### 3.1 Models with two orbiting MBHs in the galactic plane

Fig. 1a shows the gas density in the galactic plane for model 17, in which two  $10^7 M_\odot$  MBHs are orbiting in the plane of the galaxy. The wave pattern stabilizes at about 60 Myrs and there are no significant changes after this time. In Table 1 this pattern is referred to as 'stable 4-arm'. The two very dark regions indicate high densities of gas captured by the two orbiting MBHs. At this radius (1 kpc) the two MBHs drive a strong two-armed spiral. Inside the radius of about 600 pc the two-armed spiral changes into a spectacular four-armed spiral. The maximum density excess in the arm of the four-armed spiral is about 11% at a radius of 260 pc. There is a larger density excess at radii smaller than 100 pc, but the values presented here and in Table 1 are measured for radii larger than 100 pc, since spiral structure of smaller extent is unlikely to be resolved in observed galaxies. Fig. 1b shows that the four-armed wave pattern continues to the innermost parsecs of the galaxy and that it winds tightly around the centre. The formation of the spiral indicates that the waves propagate towards the centre of the disc, and in our model they are reflected from the inner boundary of the grid. The reflected waves interfere with the incoming ones, but because they geometrically diverge, they are quickly weakened as they move away from the boundary.

Radial and tangential density profiles for model 17 are shown in Fig 2. The radial plot indicates that between the radii of 50 pc and 0.4 kpc the wave pattern is rather uniform with a maximum density of about  $10.5 M_\odot \text{ pc}^{-2}$  and a minimum density of about  $9.5 M_\odot \text{ pc}^{-2}$ . Inflow makes the density larger at smaller radii. The plot of the tangential density profile shows that the multiplicity of the wave pattern is clearly four and the amplitude of all four arms is about the same.

The density contrasts and the morphologies for other models are given in Table 1. It is useful to compare model 17 to models 14 and 18, where the masses of the orbiting MBHs are  $10^6 M_\odot$  and  $10^8 M_\odot$  respectively. The  $10^6 M_\odot$  MBHs are too small a perturbation to generate density waves with a significant amplitude, and the density excess in the spiral arms for the  $10^8 M_\odot$  MBH model is just below 30%. The values of density excess in all three models

**Table 1.** 29 models with their parameter values and extracted characteristics: (1) model name, (2) number of orbiting MBHs, (3) inclination of the MBH's orbit with respect to the galactic plane, (4) logarithm of the mass of the MBH in  $M_{\odot}$ , (5) softening in Plummer's formula for orbiting MBHs, (6) central gas morphology and stability of wave pattern (for details see Section 3), (7) maximum arm-interarm density ratio (density measured in  $M_{\odot} \text{pc}^{-2}$  at radii larger than 100 pc) and its corresponding density excess in spiral arms in brackets (global values are given if no structure) and (8) time at which densities were measured.

Name (1)	Number of MBHs (2)	i (3)	log(M) (4)	$r_s$ [pc] (5)	Morphology (6)	Max Density Ratio (7)	Time [Myr] (8)
1	1	0	6	100	disturbed 3-arm	10.02/9.94 (0.8%)	100
2	1	0	7	10	disturbed 3-arm	10.58/9.65 (9.6%)	100
3	1	0	7	50	disturbed 3-arm	10.53/9.45 (11.4%)	100
4	1	0	7	100	disturbed 3-arm	10.58/9.79 (11.9%)	100
5	1	0	8	100	disturbed 3-arm	14.41/8.67 (66.2%)	100
6	1	45	6	100	no structure	10.01/9.98 (0.3%)	100
7	1	45	7	10	variable 3-arm	10.10/9.86 (1.9%)	75
						10.10/9.86 (2.4%)	100
8	1	45	7	50	variable 3-arm	10.06/9.91 (1.5%)	75
						10.05/9.92 (1.3%)	100
9	1	45	7	100	variable 3-arm	10.04/9.93 (1.1%)	75
						10.12/9.80 (3.2%)	100
10	1	90	6	100	no structure	10.01/9.97 (0.4%)	100
11	1	90	7	10	variable 3-arm	10.07/9.82 (2.5%)	72
						10.14/9.79 (3.5%)	100
12	1	90	7	50	variable 3-arm	10.11/9.86 (2.5%)	72
						10.13/9.82 (3.1%)	100
13	1	90	7	100	variable 3-arm	10.15/9.82 (3.3%)	72
						10.07/9.89 (1.8%)	100
14	2	0	6	100	stable 4-arm	10.04/9.95 (0.9%)	100
15	2	0	7	10	stable 4-arm	10.53/9.50 (10.8%)	100
16	2	0	7	50	stable 4-arm	10.66/9.55 (11.0%)	100
17	2	0	7	100	stable 4-arm	10.61/9.53 (11.3%)	100
18	2	0	8	100	stable 4-arm	11.60/8.95 (29.6%)	100
19	2	45	6	100	no structure	10.00/9.97 (0.3%)	100
20	2	45	7	10	stable 2-arm	10.26/9.64 (6.4%)	100
21	2	45	7	50	stable 2-arm	10.18/9.70 (4.9%)	100
22	2	45	7	100	stable 2-arm	10.12/9.81 (3.1%)	100
23	2	45	8	100	stable 2-arm	11.40/9.12 (25.0%)	100
24	2	75	7	100	variable 4-arm	10.07/9.91 (1.6%)	100
25	2	90	6	100	no structure	10.00/9.97 (0.3%)	100
26	2	90	7	10	variable 4-arm	10.00/9.93 (1.4%)	58
						10.14/9.82 (3.2%)	89
27	2	90	7	50	variable 4-arm	10.06/9.92 (1.4%)	58
						10.12/9.80 (3.2%)	89
28	2	90	7	100	variable 4-arm	10.08/9.92 (1.61%)	58
						10.12/9.85 (2.7%)	89
29	2	90	8	100	variable 4-arm	10.72/9.51 (12.7%)	58
						11.46/8.66 (32.3%)	89

indicate that it appears proportional to the MBH mass in the range between  $10^6$  and  $10^7 M_{\odot}$  (and perhaps below it), but it increases more slowly for masses above  $10^7 M_{\odot}$ , most likely because of reaching the non-linear regime.

Parameters of models 15–17 are identical except for the softening in Plummer's formula for the MBH. The density contrast appears to increase slightly as the softening value decreases making the images sharper. However the effect is small and we do not analyze it any further.

### 3.2 Models with two MBHs in orbits inclined to the galactic plane

Each of the models 20, 24 and 26 has two  $10^7 M_{\odot}$  MBHs orbiting in a plane inclined to the galactic plane. The inclination angle is

$45^\circ$ ,  $75^\circ$  and  $90^\circ$  respectively. A stable two-arm spiral within a set of rings is generated in model 20. The maximum density excess in the spiral arms is 6.4% at a radius of 170 pc. The rings outside the spiral arms are disturbed periodically by the motion of the orbiting MBHs. In model 24 a four-arm spiral is seen. It has a maximum density excess of only 1.6% and the density contrast changes considerably along the spiral arms, with the spiral morphology evolving in time. In model 26 the waves generated in gas produce structures that change in time. At 60 Myrs a uniform four-arm spiral is seen with a density contrast of 1.4%. This subsequently evolves into a four-armed structure that has two strong arms and two weaker arms. Its density contrast at about 90 Myrs is 3.2%. In Table 1 we refer to this structure as 'variable 4-arm'.

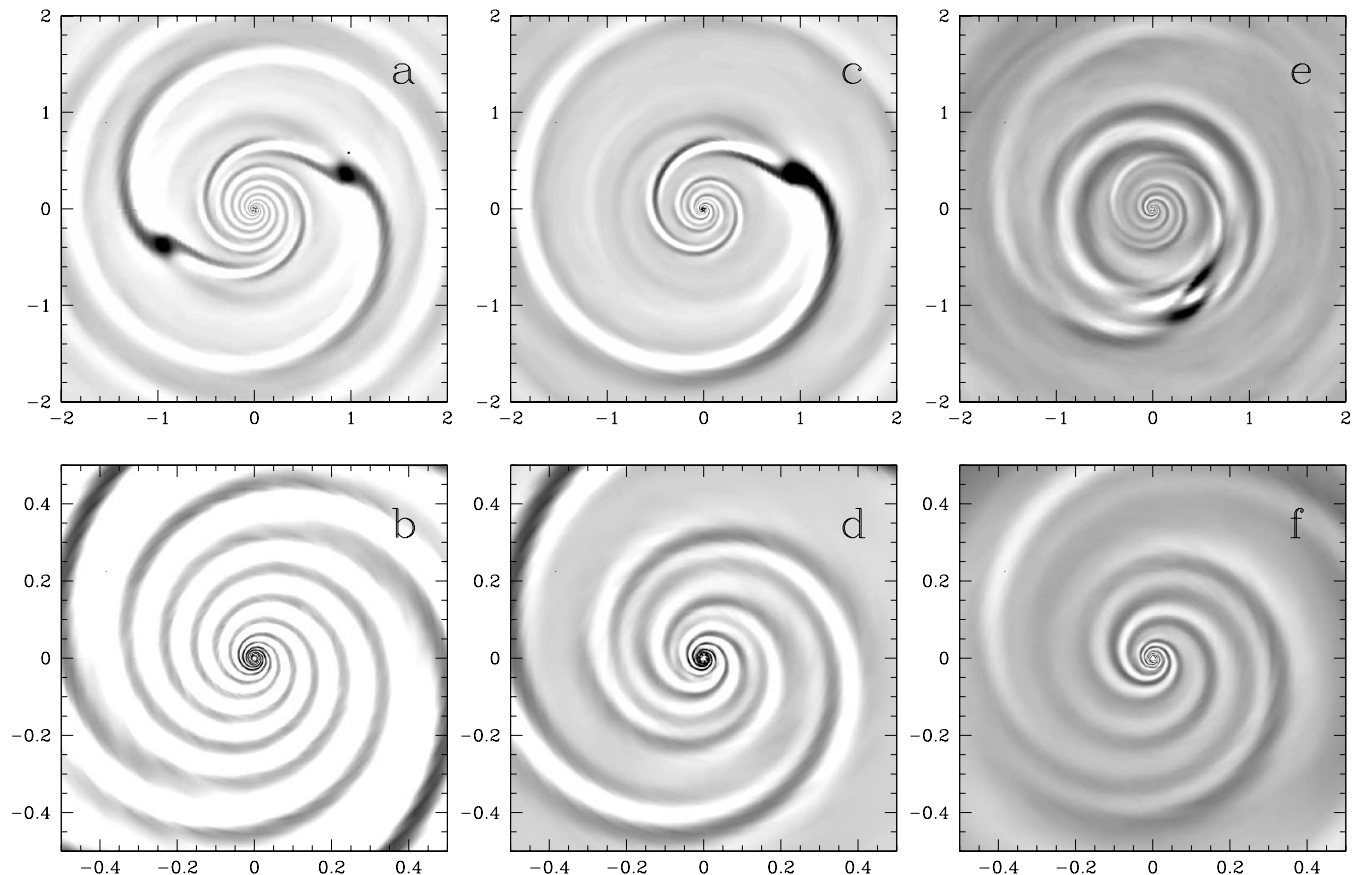


**Figure 1.** a) The density of gas in the galactic plane in greyscale for model 17, which has two  $10^7 M_{\odot}$  MBHs with softening of 100 pc orbiting in the plane of the galaxy, seen at 100 Myrs. c) Same as for a) but for model 4, which has one  $10^7 M_{\odot}$  MBH with softening of 100 pc orbiting in the plane of the galaxy, seen at 100 Myrs. e) same as a) but for model 11 which has one  $10^7 M_{\odot}$  MBH with softening of 10 pc orbiting perpendicular to the plane of the galaxy, seen at 70 Myrs. Panels b), d) and f) show details for the central kpc of corresponding panels a), c) and e). Units on the axes are in kpc.

### 3.3 Models with one orbiting MBH in the galactic plane

In simulations with one MBH orbiting in the galactic plane, the gas morphology is vastly changed. Fig. 1c shows gas density in model 4. The single very dark region represents a high density of gas captured by the MBH orbiting in the galactic plane. This MBH drives a strong single-armed spiral at neighbouring radii. However, at radii of less than 450 pc a more complex behaviour is seen. There are three spiral arms emerging from the galactic centre with a maximum density excess in the arms of 12%. However, unlike in model 17 with two MBHs, the density contrast here varies along the spiral arms (Fig. 2, top-left panel) and at some radii a fourth arm appears, like at radius about 200 pc at negative  $y$  coordinates. The azimuthal density profile at most radii shows three maxima, one of which is broad, with two peaks (Fig. 2, right panel). This may be interpreted as a four-arm spiral, but contrary to the profile of a clear four-armed spiral in model 17, the spacing of the peaks is uneven here. Thus the wave pattern is closer to a disturbed three-armed spiral and it is classified as such in Table 1. We note however, that inside the radius of 50 pc the pattern consistently shows three clear spiral arms of equal amplitude, as indicated by the dotted line in the right panel of Fig. 2. Fig. 1d shows that the spiral pattern propagates to the centre of the galaxy, and that it tightly winds around it.

### 3.4 Models with one MBH in orbit inclined to the galactic plane

Model 11 (Fig. 1 e,f) has a single MBH in an orbit perpendicular to the galactic plane. The basic difference between this model and model 4, with a MBH in the galactic plane is that the strong single-arm spiral present in the latter is missing now. Now, the orbiting MBH that passes through the galactic plane, causes a disturbance to what otherwise looks like a set of rings of radii similar to that of the MBH's orbit. The wave pattern now becomes more time dependent and the disturbance in the rings is reinforced each time the black hole passes through the plane. However, the wave pattern generated in the central region of the galaxy, within a radius of about 300 pc, does not show periodic changes related to the orbiting MBH, and for most of the run it is importantly still a three-armed spiral. The maximum density excess in the spiral arms is about 3% at radii above 100 pc, but it gets larger further in, reaching 5% and more. Towards the end of the run, at 100 Myrs, this pattern evolves into a two-arm spiral with a weak third arm. We refer to this as a 'variable 3-arm' spiral in Table 1.

Model 7 has a single MBH orbiting in a plane inclined at  $45^{\circ}$  to the galactic plane. The morphology in this model is the same

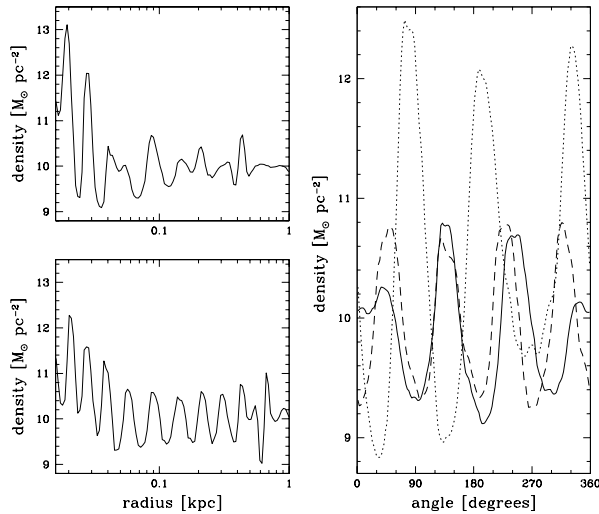


**Figure 2.** **Left:** Gas density profiles as a function of radius, taken at 100 Myrs at an angle of  $80^{\circ}$  clockwise with respect to the positive  $x$ -axis. The top panel represents model 4 with one orbiting MBH and the bottom panel model 17 with two orbiting MBHs. **Right:** Gas density profiles as a function of angle taken at 100 Myrs. The solid and dotted curves mark the profiles for model 4 taken at a radius of 71 pc and 29 pc, respectively. The dashed curve is the profile for model 17 taken at a radius of 71 pc.

as seen in model 11, but the density contrast in the spiral is weaker than in model 11, while it is stronger in the rings outside the spiral.

#### 4 INTERPRETATION

We expect that the spiral structure in gas in the centres of galaxies, observed in our models, is the consequence of waves generated by orbiting MBHs. In the linear theory of density waves in gas resonance-excited by a rotating asymmetry in the potential, in the absence of self-gravity (Goldreich & Tremaine 1978, 1979), an  $m$ -arm spiral is generated at the resonance, where the epicyclic frequency  $\kappa$  is integer  $m$  times larger than the orbital frequency  $\Omega$  in the frame rotating with the asymmetry. Thus the condition for a resonance inside the orbit of the MBH is  $\Omega - \kappa/m = \Omega_p$ , where  $\Omega_p$  is pattern speed of the asymmetry — in our case the angular velocity of the MBH. Spirals generated by such resonances are confined within their radii.

In the first part of this work models with two orbiting MBHs were constructed. Although such a setup is unphysical, the forcing here is bisymmetric, like in the well established models of gas flow in barred galaxies. By comparing our results to those models we can make first steps in the interpretation of the morphology that we observe. Because of bisymmetry, gravitational potentials in both cases do not contain odd modes, hence they cannot trigger odd-multiplicity spirals, which is confirmed by the models. However, a four-arm spiral is seen in the central parts of the galaxy in our models, contrary to a two-arm spiral which appears in models with bars. Why does a pair of orbiting MBHs generate a four-armed spiral while a two-armed spiral is observed in the case of a bar? To explain this difference, we made plots of  $\Omega - \kappa/m$  against radius for various  $m$  for the gravitational potential used in our models. In the case of two MBHs orbiting in the galactic plane the  $m = 4$  resonance is located at 620 pc. This agrees remarkably well with the distance from the centre, at which the four-arm spiral ends in

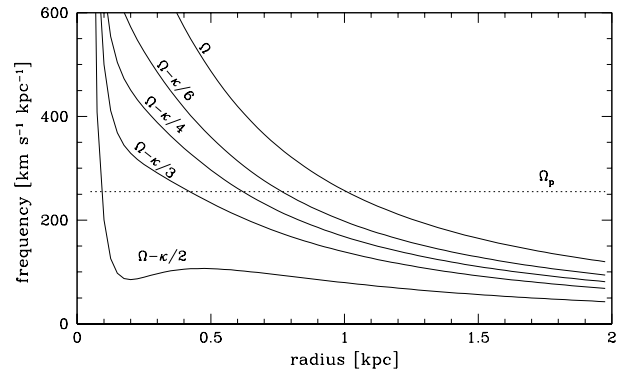


**Figure 3.** Frequency-radius diagram for the gravitational potential used in our models.  $\Omega - \kappa/m$  curves are represented by solid lines. The dotted line marks the pattern speed  $\Omega_p$  corresponding to the angular velocity of a MBH placed at a radius of 1 kpc.

Fig. 1a. In the linear theory a four-arm spiral should be generated by a  $m = 4$  resonance and propagate inwards, and the models indicate that this mechanism indeed operates in galactic centres: the spiral density waves are being driven by the MBHs that constitute an asymmetric perturbation in the galactic potential.

However, in the gravitational potential of our models an  $m = 2$  resonance is present at the radius of 93 pc (Fig. 3). Why is a two-armed spiral not generated there? Here understanding can be gained by comparing the ratio of the tangential to radial components of the gravity force between our model with orbiting MBHs, and a potential of a weak oval, which is known to generate two-arm spirals (Maciejewski 2004b). Contour plots for these ratios are presented in Fig. 4. Note that in the case of the oval, the maximum tangential forcing is well inside the corotation radius. On the other hand, in the case of an orbiting MBH the tangential forcing is largest at corotation, and it quickly loses its strength at smaller radii, where resonances are located. In the case of a weak oval (Fig. 4, right panel) a force ratio of 0.006 at the  $m = 2$  resonance is sufficient to drive the two-arm spiral mode. This mode prevails despite the fact that at the position of the  $m = 4$  resonance the force ratio is about 50% larger at 0.01. On the other hand, in the case of two orbiting  $10^8 M_{\odot}$  MBHs (Fig. 4, left panel) the force ratio at the  $m = 2$  resonance is 0.001 whereas at the  $m = 4$  resonance it is 0.014. Reduction of tangential forcing at the  $m = 2$  resonance by a factor of 14 is likely the reason why the two-arm mode is not observed in our models. Relatively weak tangential forcing at low multiplicity modes is an inevitable feature of potentials with orbiting bodies, as Fig. 4 indicates.

Our interpretation of structures observed in models with two orbiting MBHs was aided by the existing work on bisymmetric potentials. After learning from this case, we move to the physically relevant situation, where there is one orbiting MBH, corresponding to the most massive MBH in the distribution predicted by Islam et al. (2003, 2004a). In this case, the gravitational potential is no longer bisymmetric, so the presence of a spiral with an odd number of arms is not unexpected. However, in the linear theory the  $m = 1$  mode cannot be driven, because  $\Omega - \kappa$  is always negative, hence there is no  $m = 1$  resonance. The single arm seen in our models at radii close to the MBH (Fig. 1c) is a nonlinear effect, or an interference of higher-order modes (Ogilvie & Lubow 2002). The next odd mode,  $m = 3$ , generates a three-armed spiral. The  $m = 3$  resonance is found to be at the radius of 422 pc,

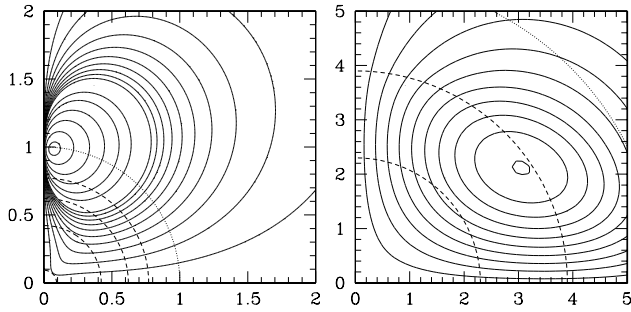


**Figure 4.** The solid lines mark contours of constant ratio of the tangential to radial components of the gravity force. The case of our potential with a  $10^8 M_{\odot}$  MBH softened at 100 pc, placed on the  $y$ -axis at 1 kpc is presented in the left panel. An oval distortion used by Maciejewski (2004 b) is shown in the right panel. The contour values, from outer to inner, are: 0.001 to 0.01 at 0.001 intervals, then 0.015, 0.02, 0.03, 0.05, 0.1 and 0.2. The dashed curves represent the positions of the resonances. On the left panel, the  $m = 2$  resonance is at 93 pc,  $m = 3$  at 422 pc,  $m = 4$  at 621 pc and  $m = 6$  at 771 pc. The dotted line marks the corotation at 1 kpc. On the right panel, the  $m = 2$  resonance is at 2.3 kpc, the  $m = 4$  at 3.9 kpc and the corotation at 5.9 kpc is marked by the dotted line. The units on the axes are in kpc.

and this agrees very well with the extent of the three-arm spiral observed in the representative model 4. However, the three-arm spiral seen in this model is not completely uniform, and it exhibits some even-multiplicity structure. From Fig. 4 we see that the maximum tangential to radial force ratio at the  $m = 3$  resonance is 0.005, while at  $m = 4$  resonance it is 0.014, less than three times larger. Thus one should expect contributions to the structure in our models from even-multiplicity modes. This analysis shows that the linear theory is applicable also to the case of a single orbiting MBH and that this MBH is the driving perturbation in this case.

## 5 DISCUSSION

### 5.1 Upper mass limit and the number of orbiting MBHs

The work reported here investigated the response of gas in the central parts of a galactic disc to the periodic forcing from possibly most massive orbiting MBHs. Evolutionary merging scenarios predict that MBHs as massive as  $10^7 M_{\odot}$  can form in galactic halos (Islam et al 2003, 2004a). Many of these most massive MBHs will spiral into the nucleus within the Hubble time because of dynamical friction. From formula (7-26) in Binney & Tremaine (1987) we get that a  $10^6 M_{\odot}$  MBH, which formed at a distance of 1 kpc from the galactic centre, will spiral in within less than 10 Gyr. Since the friction timescale is roughly inversely proportional to the orbiting mass, the upper mass limit for a MBH formed at 1 kpc and still residing there is below  $10^6 M_{\odot}$ . However, MBHs were likely to form at larger radii. Since the friction timescale is also proportional to the square of the initial radius, a  $10^7 M_{\odot}$  MBH which formed at a 5 kpc radius will need about 20 Gyr to spiral in, out of which it will take almost 1 Gyr to move through the inner kpc. This last value is still much larger than the orbital period at 1 kpc, which is about 20 Myr. Thus a  $10^7 M_{\odot}$  MBH spends enough time at the radius of 1 kpc to generate the structure in gas analyzed in this work. On the other hand, a  $10^8 M_{\odot}$  MBH will need only less than 100 Myr to spiral in from 1 kpc to the galactic centre, so there will be

no steady state gas response. Anyway, such accretion events will be too rare to be observed.

There are other constraints on the upper mass of the orbiting MBHs that sink to the galactic centre through dynamical friction most likely contribute to the formation of a SMBH there. Unacceptable build-up of this central object would occur if the halo were to consist of MBHs with all masses higher than  $\sim 3 \times 10^6 M_{\odot}$  (Xu & Ostriker 1994). Also stellar velocity dispersion in galactic discs would increase beyond the observed values if bodies orbiting in the halo were too massive. For a galaxy like the Milky Way it would happen when all MBHs were to have mass larger than  $\sim 3 \times 10^6 M_{\odot}$  (Carr & Sakellariadou 1999). This upper mass limit can be pushed up for more massive galaxies. From all the constraints above, the upper mass limit for orbiting MBHs should be somewhere in the range of a few times  $10^6 M_{\odot}$  (see also van der Marel 2004 for a review).

An important limitation of Islam et al. (2004a) simulations, from which we got the predicted population of orbiting MBHs, was that their orbital calculations could not be followed down to arbitrarily small radii. If the orbiting MBH reached a distance of 3 kpc from the centre, it was assumed that it had ‘fallen in’. Thus all MBHs that were less than 3 kpc away from the centre were assumed to merge efficiently with one another and with the central SMBH. This is quite a severe limitation considering that the Schwarzschild radius for a  $10^8 M_{\odot}$  SMBH is only about  $400 R_{\odot}$ . Simulations by Milosavljević & Merritt (2001) indicate that the separation between two MBHs at the centres of merging galaxies remains approximately constant at around 0.3 kpc for Milky Way sized galaxies for a significant time before the MBHs form a hard binary. It is therefore conceivable that MBHs could orbit around the centres of galaxies at radii much smaller than 3 kpc, and the number of orbiting MBHs should therefore be larger than what is indicated by Islam et al. (2004a).

### 5.2 Detectability of orbiting MBHs through structures in gas

Phenomena studied in this work are similar to tidal interactions in protoplanetary systems (e.g. Lin & Papaloizou 1993, Bryden et al. 1999), although there are significant differences between the two. Discs considered here are not Keplerian, and their interstellar medium is best described by warm gas (e.g. Englmaier & Gerhard 1997). Orbiting MBHs considered in this work spiral into the galactic centre within few tens of their orbital period, and therefore features observed in our models are relevant only if they occur on similar timescale. For this reason we do not expect in galactic discs a gap-opening, similar to that occurring in protoplanetary discs after a few hundreds of protoplanet’s orbits. Moreover, orbiting MBHs are not confined to the galactic plane, and off-plane MBHs are much less efficient in gap-opening in the disc. The common feature of protoplanetary discs and galactic discs with MBHs in the disc plane, the one-arm spiral that accompanies the orbiting body, is also absent in the case of MBHs not confined to the galactic plane. However, the spiral structure created in gas in the central parts of the galactic discs, at radii at least twice smaller than the orbital radius of the MBH, is of similar strength for MBHs orbiting in the disc plane and out of the plane. This is the structure on which we focus in this paper.

MBHs not confined to the galactic plane will generate vertical modes in the gaseous disc. We expect these modes to be of similar magnitude to the horizontal modes, which are weak and remain within the linear regime. Thus the full solution is likely to be a linear superposition of the modes, out of which we consider here

only those propagating in the disc plane. These modes are most important when interpreting the observed nuclear morphology in galaxies. However, full three-dimensional simulations, beyond the scope of this paper, are required to explore the possible coupling of horizontal and vertical modes.

Will orbiting MBHs of the highest permissible mass generate spiral structure in gas that is observable with currently available techniques? Dusty filaments that have been discovered recently in the centres of galaxies (e.g. Martini et al. 2003, Prieto, Maciejewski & Reunanen 2005) have luminosity lower from their surroundings by 5 – 10%. Our models indicate that density excess in the spiral pattern generated by a  $10^7 M_{\odot}$  MBH ranges from 12% for the MBH orbiting in the galactic plane to 3% for the off-plane MBH. Thus structures in gas generated by MBHs of this mass should be detectable, especially for MBHs orbiting close to the galactic plane. On the other hand, the density excess in models with an orbiting  $10^6 M_{\odot}$  MBH is only about 1%. A pattern of this strength will most likely remain undetected, and it probably will be overridden by random density fluctuations in centres of galaxies.

In the models constructed in this work, we assumed that the MBHs are orbiting in the otherwise rigid potential. One should note though that the MBH masses considered here are large enough to generate a significant response in the distribution of stars. Appropriate implementation of this effect requires full N-body simulations, which are beyond the scope of this paper, but it is clear that the stellar response will amplify waves driven in gas by the orbiting MBH. This should enable detections of MBHs with slightly lower masses, down to a few times  $10^6 M_{\odot}$ . On the other hand, the mass of the central SMBH constitutes only 0.65% of the total mass encircled by the MBH's orbit, hence no significant reflex motion of the central SMBH is expected.

Considerations above lead to an interesting conclusion, namely that orbiting MBHs of the highest permissible mass generate phenomena in gas that are right on the verge of detection with current observational techniques. This is not only encouraging, but it also ensures that in a given galaxy only one exceptionally massive MBH (if any at all) will generate structure in gas, and this structure therefore should be coherent. If there was strong response in gas to orbiting MBHs of masses orders of magnitude smaller than the upper mass limit, then the structure in gas would be incoherent, especially that gas response becomes nonlinear just one order of magnitude above the pattern detection limit (Section 3.1).

One of our main conclusions is that one orbiting MBH generates a three-arm spiral in gas in the central regions of the galactic disc. Although one observation in the near-IR does not constitute a sample of any sort, it is suspicious that the dusty filaments in the centre of NGC 1097 form a three-arm spiral inside 300 pc radius, even if bisymmetry prevails at larger radii (Prieto et al. 2005). This three-arm spiral finds no satisfactory explanation, and further observations of centres of galaxies in the near-IR are needed to establish how common it is.

### 5.3 Other methods to detect orbiting MBHs

If orbiting MBHs accrete gas, they can be sources of X-ray emission. Any compact object with X-ray luminosity higher than the Eddington limit for isotropic accretion onto a stellar-mass black hole ( $L_x \geq 10^{38} \text{ erg s}^{-1}$ ) is known as an ultraluminous X-ray source (ULX). It has been suggested (Kaaret et al. 2001) that a population of MBHs could account for some fraction of the ULXs. However, emission from accreted interstellar medium (Bondi-Hoyle accretion) is insufficient to account for the observed

luminosity (e.g. King et al. 2001), and gas has to be present on site, either in a binary system or in baryonic cores. Both scenarios have problems though, since there is no known evolutionary path that produces a binary of the characteristics required by the first scenario, while MBHs which form by merging of remnants of Population III stars may be stripped by now of their baryonic cores in the second scenario.

Compact objects, like orbiting MBHs, can be detected through microlensing. The lensing duration scales as a square root of the lens mass, with a microlensing event caused by a lens of solar mass lasting about 130 days. Therefore even with long-duration events, only the low end of the mass spectrum of orbiting MBHs can be explored (van der Marel 2004).

Formation of MBHs at high redshift can be probed in the future with gravitational waves, which are released by the initial collapse of Population III stars into MBHs, and by subsequent mergers of MBHs. There could be as many as  $10^4 - 10^5$  gravitational wave events per year that may fall within the sensitivity limits of the proposed Laser Interferometer Space Antenna (LISA) gravitational wave observatory (Islam, Taylor & Silk 2004b). Observations of gravitational wave events could be used to constrain the merger history of the MBHs and to provide improved limits on their abundances. The collapse of the first stars into MBHs may also produce gamma-ray bursts. Observing them will allow the epoch of the first star formation to be directly detected at redshifts larger than twenty.

## 6 CONCLUSIONS

This paper was based on the innovative idea that orbiting MBHs could produce a signature pattern in the gas that may be used to identify them. The main result of this study is that a three-armed spiral is generated in gas when a single MBH orbits around the galactic centre. This structure is the consequence of resonance-excited waves in gas. Only MBHs at the very end of the upper range of masses permitted by dynamical constraints and evolutionary scenarios, *i.e.* with masses nearing  $10^7 M_{\odot}$ , are capable to generate structure in gas with density contrast high enough to be observed with current techniques. However, given that there are not many techniques that could assure detection of high-mass orbiting MBHs, the signature proposed here might be well worth pursuing.

## ACKNOWLEDGEMENTS

We would like to thank Prof. Joe Silk for bringing to our attention the idea that very massive black holes may be orbiting in galaxies. We thank the anonymous referee for useful comments on the similarity of our work to that on protoplanetary systems. This work was partially supported by the Polish Committee for Scientific Research as a research project in the years 2004–2006.

## REFERENCES

- Abel T., Anninos P., Norman M. L., Zhang Y. 1998, *ApJ*, 508, 51
- Abel T., Bryan G., Norman M., 2000, *ApJ*, 540, 39
- Athanasoulas E., 1992, *MNRAS*, 259, 345
- Binney J., Tremaine S., 1987, *Galactic Dynamics* (Princeton: Princeton Univ. Press)
- Bryden G., Chen X., Lin D.N.C., Nelson R.P., Papaloizou J.C.B., 1999, *ApJ*, 514, 344
- Carr B. J., Sakellariadou M., 1999, *ApJ*, 516, 195

- Englmaier P., Gerhard O., 1997, MNRAS, 287, 57  
Goldreich P., Tremaine S., 1978, ApJ, 222, 850  
Goldreich P., Tremaine S., 1979, ApJ, 233, 857  
Islam R. R., Taylor J. E., Silk J., 2003, MNRAS, 340, 647  
Islam R. R., Taylor J. E., Silk J., 2004a, MNRAS, 354, 427  
Islam R. R., Taylor J. E., Silk J., 2004b, MNRAS, 354, 629  
Kaaret P., Prestwich A. H., Zezas A. L., Murray S. S., Kim D.-W., Kilgard R. E., Schlegel E. M., Ward M. J., 2001, MNRAS, 321, L29  
King A. R., Davies M. B., Ward M. J., Fabbiano G., Elvis M., 2001, ApJ, 552, L109  
Lin D. N. C., Papaloizou J. C. B., 1993, in Protostars and planets III, eds. E.H. Levy, J.I. Lunine (Univ. Arizona Press, Tucson), 749  
Lindblad P. O., Jörsäter S., 1981, A&A, 97, 56  
Maciejewski W., 2004a, MNRAS, 354, 883  
Maciejewski W., 2004b, MNRAS, 354, 892  
Madau P., Rees M. J., 2001, ApJ, 551, L27  
Martini P., Regan M. W., Mulchaey J. S., Pogge R. W., 2003, ApJS, 146, 353  
Milosavljević M., Merritt D., 2001, ApJ, 563, 34  
Ogilvie G.I., Lubow S.H., 2002, MNRAS, 330, 950  
Piner B. G., Stone J. M., Teuben P. J., 1995, ApJ, 449, 508  
Prieto M. A., Maciejewski W., Reunanen J., 2005, AJ, 130, 1472  
van der Marel R. 2004, in Coevolution of Black Holes and Galaxies, ed. L.C. Ho (Cambridge: Cambridge Univ. Press), 37  
Xu G., Ostriker J. P., 1994, ApJ, 437, 184